STRENGTH OF LATERAL-TORSIONAL BUCKLING OF A COMPOSITE STEEL BEAM SUBJECTED TO REVERSE CURVATURE BENDING

Satoshi KITAOKA

Nippon Steel Corporation Futtsu, Japan kitaoka.7pn.satoshi@jp. nipponsteel.com

Satoru HIROSHIMA

Nippon Steel Corporation Futtsu, Japan hiroshima.kp9.satoru@jp. nipponsteel.com

Keiichi TAKADA

Retired from Nippon Steel Corporation Tokyo, Japan n1000835kt@feel.ocn.ne.jp

Ryoichi KANNO

Nippon Steel Corporation Futtsu, Japan kanno.kx4.ryoichi@ jp.nipponsteel.com

Koji HANYA

Nippon Steel Corporation Futtsu, Japan hanva.rs9.koji@jp. nipponsteel.com

Fumihisa YOSHIDA

Daiwa House Industry Co., Ltd. Nara, Japan fumihisa@daiwahouse.jp

ABSTRACT

Design guidelines for lateral-torsional buckling of I-shaped steel beams have been well established, but those of a composite beam consisting of an I-shaped beam and a floor slab have not been sufficiently understood. It is especially true for a beam subjected to reverse curvature bending, where the top flange is continuously restrained with a slab but the bottom flange may still buckle laterally. Although several strength formulae have been derived, as far as the authors know, the restraining effect is not widely considered as a common practice, partly due to lack of behavioral data available. Therefore, in this study, three sub-assemblage specimens consisting of two box steel columns, an I-shaped beam, and a composite floor slab were tested to clarify the behavior. Then a closed-form buckling strength formula was derived for the beam based on an energy method, and the results were compared with those of finite element analyses and the test results. Overall, the restraining effects were clearly observed, and the proposed formula was found to provide reasonable strength estimates.

INTRODUCTION

There has been a substantial amount of research work on lateral-torsional buckling (called LTB hereafter) of I-shaped steel beams in steel building frames (Ziemian, 2010). Design guidelines for the strength evaluation and its bracing have been well established. However, the strength evaluation for a composite beam consisting of an I-shaped beam and a floor slab is not well understood yet. It is especially true for a composite beam subjected to reverse curvature bending, where the top flange is continuously restrained with a floor slab but the bottom flange may still buckle laterally due to the compression stress. There would be an obvious benefit especially in seismic design for eliminating bracing members when such a restraining effect of the floor is considered in design. As a result, some strength evaluation formulae have been

proposed, such as those by Wakabayashi and Nakamura (1973), Bradford and Gao (1992), Yura (1995), and Kimura and Yoshino (2011).

However, as far as the authors know, the restraining effect by the floor slab is not widely considered as a common practice in design. This is partly because of the fact that enough behavioral data on the interaction between the I-shaped beam and the floor slab are not available, resulting in insufficient resources on the strength formulae. From this background, in this study, three sub-assemblage specimens consisting of two box steel columns, an I-shaped beam, and a reinforced concrete floor slab were first tested under horizontal loading applied to the columns. Such a loading condition is typically seen in seismic design. Then, a formula for closed-form elastic buckling strength for the restrained I-shaped steel beam under various moment gradients was developed based on an energy method using newly proposed displacement functions. Comparisons of results of elastic finite element buckling analyses, the proposed formula, and a typical existing formula were made, and finally, the accuracy of the proposed formula was examined with the experimental data.

OUTLINE OF EXPERIMENTS

Sub-assemblage specimens shown in Figure 1 were fabricated and tested under a horizontal loading condition typically encountered in strong seismic and/or wind regions. The specimens were designed as a part of a moment-resisting frame seen in Japan, consisting of two square box columns, an I-shaped beam, and a reinforced concrete floor slab. The box columns were made of cold-formed (roll-formed) steel and have a length of 1620 mm and a square section with 300 mm width and 16 mm thickness. An I-shaped beam with a length of 5700 mm was welded rigidly to the columns at both its ends. At the beam—column connections, reinforcement was made with continuity plates between the beam flanges and the columns so that rigid connection can be realized. The floor slab above the beam was of reinforced concrete with 70

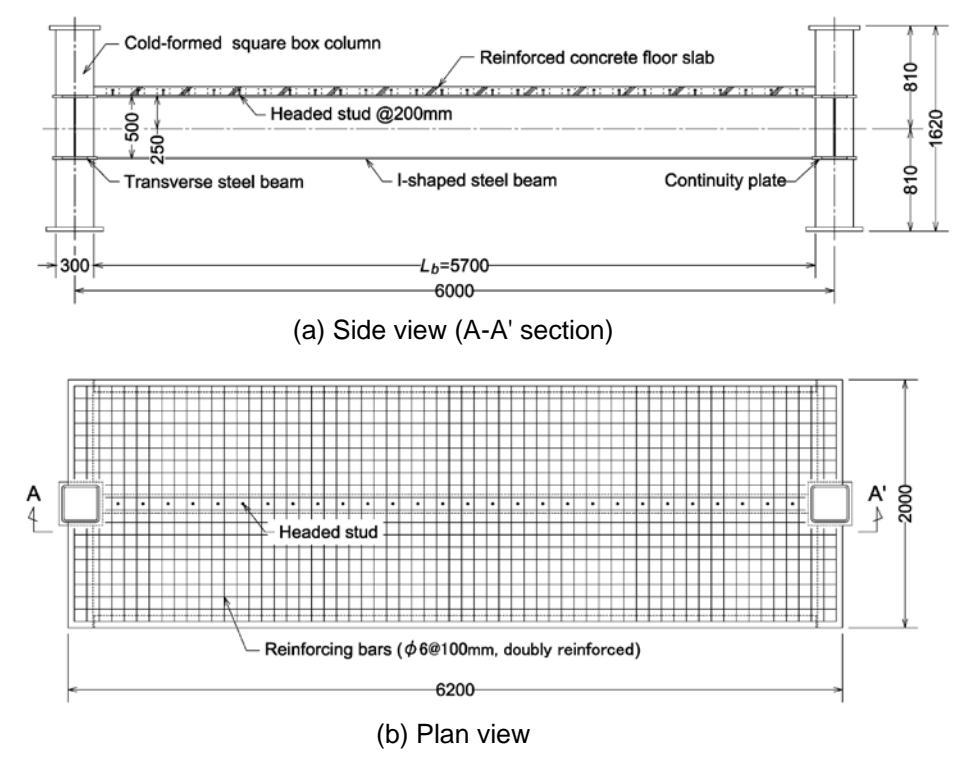


Fig. 1 – Specimen overview

mm thickness and 2000 mm width. A flat-type form deck was set beneath the floor for concrete casting. Headed steel studs with 10 mm in diameter and 50 mm in length were welded at the middle of the top flange. Following Japanese practice, the studs were arranged with a spacing of 200 mm in a row along the entire steel beam, which

Table 1 – Specimens and their beam sizes

Specimen no.	Depth (mm)	Width (mm)	Web thickness (mm)	Flange thickness (mm)
No.1	500	150	9	12
No.2	500	116	9	12
No.3	500	65	9	12

provides about one-half of the full composite action required by the AISC specification. From strong restraints by the continuity plates, columns and floor slab, it can be assumed that both twisting and warping were substantially restrained at the beam ends.

There were three specimens (Specimens No. 1 through No. 3). The experimental variable was straightforward and was only the width of the beam that significantly affects the LTB behavior. The width changed from 65 mm to 150 mm, while the height, flange thickness, and web thickness remained constant in all specimens. Geometry information for the specimens is shown in Table 1. As understood from information in the table, all the sections were categorized into a compact section. The beams were built-up sections, and the yield strengths of the steel plates used for the flange and web were 360 N/mm² and 382 N/mm², respectively. Based on a widely used Japanese design standard, strength estimates of the steel beams without the floor slab were $0.64M_p$, $0.41M_p$, and $0.17M_p$ for Specimens No. 1 through No. 3, respectively, where M_p is the plastic moment. As seen, no specimens would reach M_p if the slab restraining effect was not taken into account.

The test set-up is shown in Figure 2. The top and bottom parts of the two columns were pinsupported and two horizontal actuators were located at the top of the columns, which gave an equal displacement in the same direction. The loading provided by the actuators was controlled by displacement and the following protocol was applied: two cycles of loading at 0.5% drift angle and then monotonically increasing loading until an obvious buckling was observed.

EXPERIMENTAL RESULTS AND OBSERVATIONS

Load and displacement relationships are shown in Figure 3. The load is represented by bending moment M that acts at the ends of the beam, and the displacement is represented by the story drift angle θ , which is defined by an inclination between the upper and lower pin-supports of the columns. Since composite beams behaved differently in positive and negative bending, both

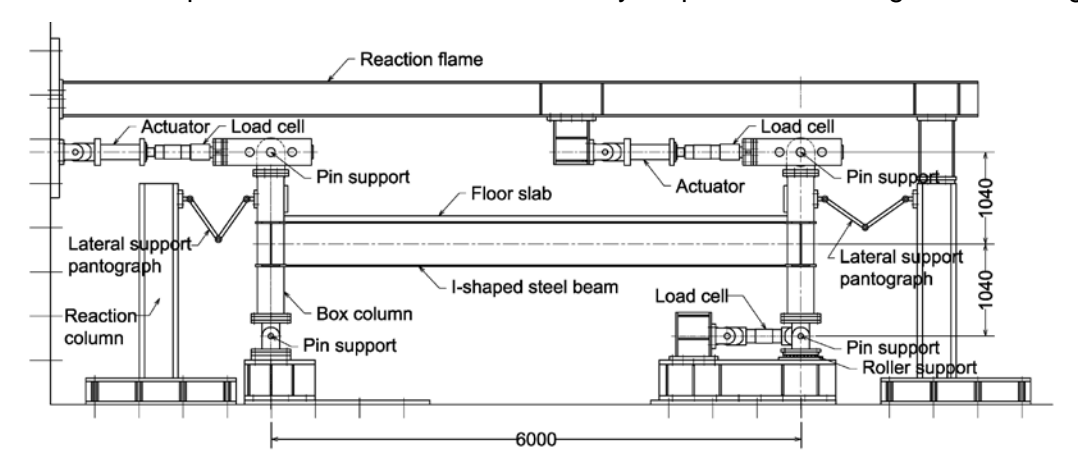


Fig. 2 – Test set-up and loading condition

relationships at positive and negative sides are shown in Figure 3. The average relationships are also indicated in the same figures with finer broken lines. From the average relationships, it can be said that the specimens were quite ductile and relatively similar to each other. They started with elastic behavior, reached the maximum strength, and then showed yielding without much strength deterioration. The figure also indicates that both stiffness and strength were apparently larger in positive bending side than in negative side because of the composite action. In the three specimens, no buckling and cracking were observed in the slabs at the cyclic loading of 0.5% drift angle.

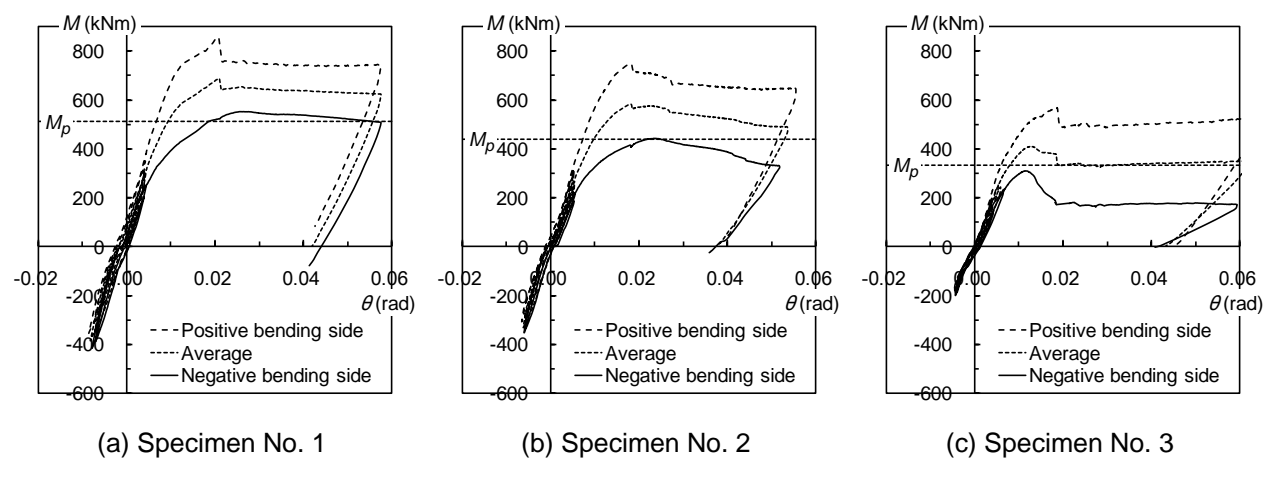


Fig. 3 – Load-displacement relationships

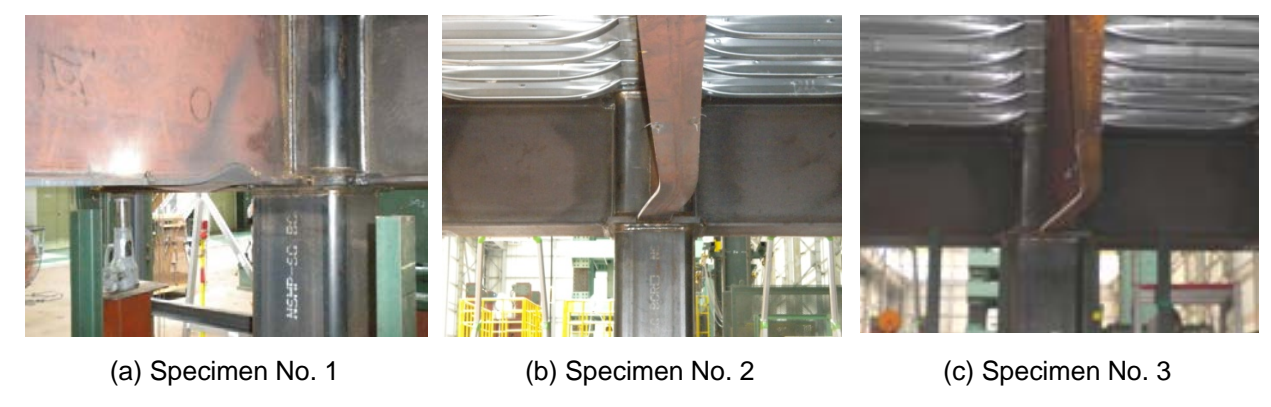


Fig. 4 –Buckling deformation observed at the negative bending side

Each specimen's behavior is described as follows: Specimen No. 1 having the widest flange showed an obvious load drop at a drift angle of around 1.9% due to concrete crushing of the slab around the column face at the positive side. Subsequently, flange local buckling occurred at a drift angle of about 2.5% as seen in Figure 4 (a), but little strength deterioration was observed until the loading was terminated. LTB did not occur in this case, instead, local flange buckling was identified as in Figure 4 (a). Specimen No. 2 showed a similar load—displacement relationship to that of Specimen No. 1. After concrete crushing was observed, buckling occurred at a drift angle of around 2.4% with LTB and slight flange local buckling as shown in Figure 4 (b). The last specimen, Specimen No. 3 also showed concrete crushing at the positive bending side and a clear LTB at a smaller drift angle of around 1.9% than those of the previous two specimens. Although concrete crushing of the floor slabs was observed in all the specimens, obvious damage was not identified around the stud connections, as seen in Figure 5.

Through the behaviors of the three specimens shown in Figure 4, it is clear that the top flange of the steel beam was completely restrained at least laterally. This demonstrated that the floor slabs had enough capability to restrain the lateral movement of the steel beams, even though the beams were not fully composite. Plastic moment strengths M_p are shown with horizontal broken lines in Figure 3, indicating that for all the specimens, the maximum strengths of the beams in the negative bending side were found around their plastic moment strengths. The strengths were $1.06M_p$, $1.00M_p$, and $0.91M_p$ for Specimens No. 1 through No. 3, respectively. Compared with the previously indicated strength estimates for those without a floor slab, substantial strength increases were found especially in Specimens No. 2. and No. 3. These observations indicate that floor slabs possess considerably strong restraining effects on the LTB of the I-shaped steel beams.





- (a) Concrete crushing around the columns
- (b) Appearance around the studs

Fig. 5 – Damage and appearance observed in and around reinforced concrete slab

EXISTING STRENGTH FORMULA

Various design formulae for LTB of I-shaped beams have been proposed. All the formulae are established primarily as a function of plastic moment strength M_p and elastic bucking strength M_{cr} . For the cases where the top flange is continuously restrained with a floor slab, as seen in the previous experiments, several LTB formulae have been proposed; for example by Wakabayashi and Nakamura (1973), Bradford and Gao (1992), Yura (1995), and Kimura and Yoshino (2011). Most of the formulae are developed based on governing differential equations or the equivalent energy equation, but their derivation is so complex that the closed-from solution is rarely possible. Therefore, existing formulae are rather approximate, established based on numerical analysis.

Among the formulae, widely recognized is the one adopted in the AISC specification (AISC, 2010), which is originally proposed by Yura (Yura, 1995). It provides the following elastic buckling strength M_{cr} :

$$M_{cr} = C_b M_{cr0} \tag{1}$$

where M_{cr0} is the elastic buckling strength for uniform bending moment, and C_b is the LTB modification factor for non-uniform moment including reverse curvature bending:

$$C_b = 3.0 - \frac{2}{3} \left(\frac{M_1}{M_o} \right) - \frac{8}{3} \left[\frac{M_{CL}}{(M_o + M_1)^*} \right]$$
 (2)

where M_o is the moment at the end of the unbraced length, which gives the largest compressive stress in the bottom flange, M_1 is the moment at the other end of the length, and M_{CL} is the moment at the middle of the length. Note that in Eqn. (2) that $(M_o + M_1)^* = M_o$, if M_1 is positive.

To obtain the design strength M_n , the elastic buckling strength M_{cr} is applied to design equations given in the AISC specification.

PROPOSED CLOSED FORM STRENGTH FORMULA

Since the existing formulae for the buckling are approximate, there might be some errors in the strength estimation. As far as the authors know, no closed-form solution is currently available for the elastic LTB strength of an I-shaped steel beam restrained by a floor slab. This is because the equation becomes so complex that only numerical solutions can solve the problem.

A closed-form solution is derived in this study based on an energy method (Rayleigh-Ritz method) by assuming rather untraditional displacement functions. Figure 6 shows a stability problem of simply supported doubly symmetric I-shaped beam whose top flange is continuously restrained laterally (a sign "X" means the lateral restraint). The beam is subjected to arbitrary end moments, where β is introduced as a parameter to express various moment gradients. At the middle of the top flange, the lateral displacement is continuously restrained, while the twist rotation is free to move. Two types of end restraint conditions are considered: torsional simple support and fixed support conditions. Composite action with floor slab is neglected.

Note on this model in Figure 6 that Bradford and Gao (1992) assumed a laterally and torsionally fixed condition at the top flange, resulting in what they called "lateral-distortional buckling." Since

it is still uncertain from a practical viewpoint whether the torsionally fixed condition is assumed, this study employs only a laterally fixed condition, which is in most cases conservative for strength evaluation.

Back to the formulation, the total potential energy is described as follows (Trahair, 1993):

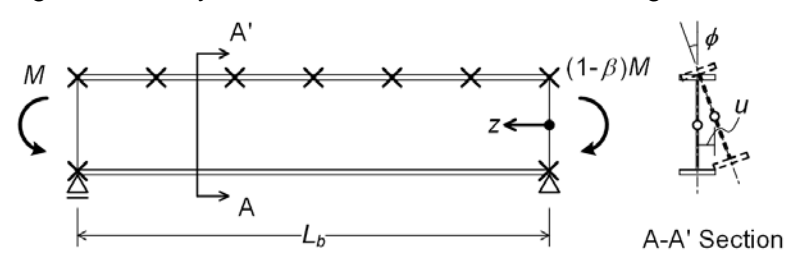


Fig. 6 - Restrained I-shaped beam with end moments

$$\Pi = \frac{1}{2} \int_{0}^{L_{b}} E I_{y} u''^{2} dz + \frac{1}{2} \int_{0}^{L_{b}} G J \phi'^{2} dz + \frac{1}{2} \int_{0}^{L_{b}} E C_{w} \phi''^{2} dz + \int_{0}^{L_{b}} M_{z} \phi u'' dz$$
 (3)

where E is Young's modulus, G is the shear modulus, I_y is the moment of inertia about the weak axes, J is the torsional constant, C_w is the warping constant, L_b is the unbraced length as shown in Figure 6, M_z is the bending moment along the beam, and u and ϕ are the horizontal displacement and twist rotation at the centroid of the beam, respectively. Neglecting the sectional distortion of the beam, the following relationship can be assumed:

$$u = \frac{d_b}{2}\phi \tag{4}$$

where d_b is the distance between the centers of the flanges. Referring to Figure 6, M_z can be expressed at a location of z as follows:

$$M_z = \left(1 - \beta + \beta \frac{z}{L_b}\right) M \tag{5}$$

Substituting Eqns. (4) and (5) into Eqn. (3), the total potential energy becomes as follows:

$$\Pi = \frac{1}{2} \frac{d_b}{L_b} \left[\frac{2\pi^2 E I_{yf} d_b}{L_b^2} B + A \frac{GJ}{d_b} - M\{(1-\beta)A + \beta C\} \right]$$
 (6)

where I_{yf} is the moment of inertia for one flange. Note that an approximate relationship of $I_y = 2 I_{yf}$ is used in the derivation from Eqn. (3). A, B and C in Eqn. (6) are functionals of ϕ shown as follows:

$$A = L_b \int_0^{L_b} {\phi'}^2 dy , \qquad B = \frac{L_b^3}{2\pi^2} \int_0^{L_b} {\phi''}^2 dy , \qquad C = \int_0^{L_b} z {\phi'}^2 dy$$
 (7), (8), (9)

As seen in Figure 6, ϕ is the only variable to describe the buckled displacement field. Here, ϕ is expressed with the following finite series such that the given boundary conditions are satisfied:

$$\phi = a_0 + \sum_{n=1}^{n} a_n \, \phi_n \tag{10}$$

where a_0 and a_n are arbitrary constants, ϕ_n is the base function, and n is the number of series. Generally, the Fourier series have been applied to Eqn. (10), but in this study, rather special functions are applied to make the closed-form solutions possible. The functions were found through try and error, and are shown for two end restraint conditions against LTB as follows:

$$\phi_n = \sin \left\{ \pi \left(\frac{z}{L_b} \right)^n \right\}$$
 for torsional simple support (no twist, free to warp) (11)

$$\phi_n = \cos \left\{ 2\pi \left(\frac{z}{L_b} \right)^n \right\}$$
 for torsional fixed support (no twist and no warping) (12)

With the above functions, enough accuracy can be obtained using only three series, i.e., n=3, whereas the number of series is considerably larger with traditional Fourier series, especially for the cases with various moment gradients. This large number of series has made the closed-form solutions quite difficult. The proposed displacement functions can describe the buckled shape more efficiently. Substituting Eqn. (10) into Eqn. (6) and applying a stationary condition in terms of a_n to Eqn. (6), a cubic equation in terms of M can be obtained as an eigenvalue problem. By solving the equation, the following closed-form elastic buckling strength M_{cr}^* can be found:

$$M_{cr}^* = \min \left\{ M^0, M^1, M^2 \right\} \tag{13}$$

where

$$M^{k} = \omega_{k}^{3} \sqrt{-\frac{q}{2} + \sqrt{\left(\frac{q}{2}\right)^{2} + \left(\frac{p}{3}\right)^{3}}} + \omega_{3-k}^{3} \sqrt{-\frac{q}{2} - \sqrt{\left(\frac{q}{2}\right)^{2} + \left(\frac{p}{3}\right)^{3}}} - \frac{A_{2}}{3}, \quad k = 0, 1, 2$$
 (14)

$$\omega_0 = \omega_3 = 1$$
, $\omega_1 = \frac{-1 + \sqrt{3}i}{2}$, $\omega_2 = \frac{-1 - \sqrt{3}i}{2}$ (15), (16), (17)

$$p = A_1 - \frac{1}{3}A_2^2$$
, $q = A_0 - \frac{1}{3}A_1A_2 + \frac{2}{27}A_2^2$, $A_j = \frac{\alpha_j}{\alpha_3}$ (18), (19), (20)

$$\alpha_0 = \begin{vmatrix} h_{11} & h_{12} & h_{13} \\ h_{21} & h_{22} & h_{23} \\ h_{31} & h_{32} & h_{33} \end{vmatrix}$$
 (21)

$$\alpha_{1} = \begin{vmatrix} g_{11} & g_{12} & g_{13} \\ h_{21} & h_{22} & h_{23} \\ h_{31} & h_{32} & h_{33} \end{vmatrix} + \begin{vmatrix} h_{11} & h_{12} & h_{13} \\ g_{21} & g_{22} & g_{23} \\ h_{31} & h_{32} & h_{33} \end{vmatrix} + \begin{vmatrix} h_{11} & h_{12} & h_{13} \\ h_{21} & h_{22} & h_{23} \\ g_{31} & g_{32} & g_{33} \end{vmatrix}$$
 (22)

$$\alpha_{2} = \begin{vmatrix} h_{11} & h_{12} & h_{13} \\ g_{21} & g_{22} & g_{23} \\ g_{31} & g_{32} & g_{33} \end{vmatrix} + \begin{vmatrix} g_{11} & g_{12} & g_{13} \\ h_{21} & h_{22} & h_{23} \\ g_{31} & g_{32} & g_{33} \end{vmatrix} + \begin{vmatrix} g_{11} & g_{12} & g_{13} \\ g_{21} & g_{22} & g_{23} \\ h_{31} & h_{32} & h_{33} \end{vmatrix}$$
 (23)

$$\alpha_{3} = \begin{vmatrix} g_{11} & g_{12} & g_{13} \\ g_{21} & g_{22} & g_{23} \\ g_{31} & g_{32} & g_{33} \end{vmatrix}$$
 (24)

$$g_{nm} = (1 - \beta)L_{nm} + \beta N_{nm}$$
 (25)

$$h_{nm} = -M_{nm} \frac{2\pi^2 E I_{yf}}{L_b^2} d_b - L_{nm} \frac{GJ}{d_b}$$
 (26)

$$L_{nm} = L_b \int_0^{L_b} \phi'_n \, \phi'_m \, dz$$
, $M_{nm} = \frac{L_b^3}{2\pi^2} \int_0^{L_b} \phi''_n \, \phi''_m \, dz$ (27), (28)

$$N_{nm} = \int_{0}^{L_{b}} z \; \phi'_{n} \; \phi'_{m} \; dz \tag{29}$$

Applying the displacement functions in Eqns. (11) and (12), L_{nm} , M_{nm} , and N_{nm} become constants by utilizing partial integration technique and numerical integration. Tables 2 and 3 show the values of L_{nm} , M_{nm} , and N_{nm} for simple support case and fixed support case, respectively.

Table 2 – Values of L_{nm} , M_{nm} , and N_{nm} for torsional simple support

	n=1, m=1	n=2, m=2	n=3, m=3	n=1, m=2	n=1, m=3	n=2, m=3
L_{nm}	4.935	6.310	8.589	3.799	2.750	6.667
M_{nm}	2.467	9.329	26.33	1.899	1.375	13.49
N_{nm}	2.467	4.935	7.402	2.802	2.489	5.604

Table 3 – Values of L_{nm} , M_{nm} , and N_{nm} for torsional fixed support

	n=1, m=1	n=2, m=2	n=3, m=3	n=1, m=2	n=1, m=3	n=2, m=3
L_{nm}	19.74	26.75	35.96	9.224	-0.2315	23.93
M_{nm}	39.48	128.8	362.8	18.45	-0.4629	165.7
N_{nm}	9.870	19.74	29.61	6.763	1.077	19.21

Eqn. (14) is known as Cardano's formula, which provides three roots. They may take real numbers and/or complex numbers, depending on the value of the discriminant $D = (q/2)^2 + (p/3)^3$. Since the real roots are meaningful, their minimum value becomes the solution for Eqn. (13), which is the buckling strength M_{cr}^* . Although the solution is expressed in a closed-form, rather bothersome calculation work is needed.

ACCURACY OF PROPOSED FORMULA

The accuracies of the proposed strength formula and Yura's formula were examined by comparing elastic finite element buckling analysis (i.e., eigenvalue analysis). Note that the comparisons made here is on elastic buckling strength, and the inelastic strength will be discussed later in this paper. Figure 7 shows a finite element (FE) model of simply supported I-shaped beam with end moments and shearing forces with flange continuously the restrained horizontally at the middle of the flange. Variables considered in the analyses included the beam end support condition for LTB, beam size, beam length L_b , and moment gradient defined by β . There were two end restraint conditions: one is torsional simple support (only sway is restrained) and another is torsional fixed support (both sway and warping are prevented). These end restraint conditions were made possible by discrete restraints given at the

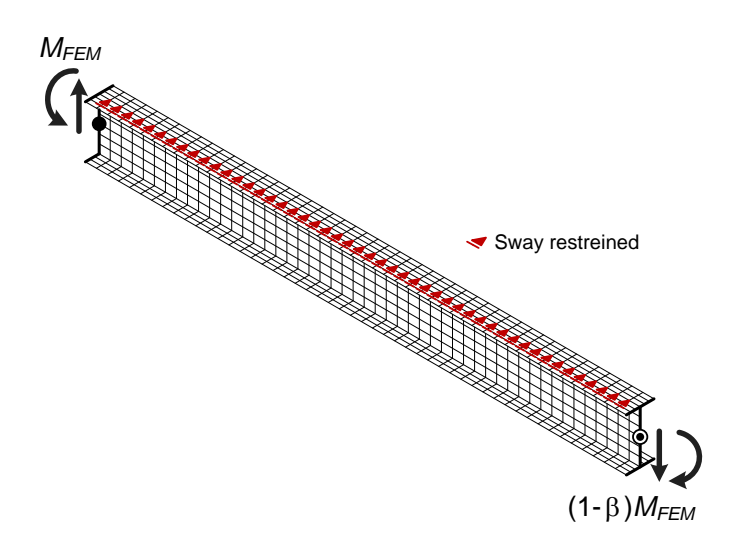


Fig. 7 – Finite element analysis model

Table 4 – Beam sizes considered in the analyses

Beam type	Depth (mm)	Width (mm)	Web thickness (mm)	Flange thickness (mm)
Case 1	400	400	13	21
Case 2	588	300	12	20
Case 3	600	200	11	17

centroids of the sections and rigid-bar addition along the sections at the beam ends. Note that as mentioned previously, the fixed support case may correspond to the experiments conducted in this study. The beam sizes considered here is shown in Table 4. Three types of beams with different widths and depths were taken into consideration. The beam length L_b was varied such that L_b/H (H is the beam depth) changes from 6 to 100 at an interval of 2. Four types of moment gradients were also considered by taking β equal to 0, 1, 2, and 3. In these moment gradients, β = 2 corresponds to an equal end moment and a double curvature bending case that is typically seen in seismic design. By combining all the variables, more than 500 cases of buckling analyses were carried out to obtain a database for the critical buckling strengths M_{FEM} .

Figure 8 shows comparisons between the FE analyses and the proposed formula given by Eqn. (13). Both simple and fixed cases are shown in Figure 8 (a) and (b), respectively. In the figure, the horizontal axis represents the non-dimensional slenderness ratio defined by $\sqrt{M_p/M_{cr}^*}$, where M_p is the plastic moment strength and M_{cr}^* is the calculated buckling strength given by Eqn. (13). Yield strength of the steel beams was assumed to be $F_y=325~{\rm N/mm^2}$. On one hand, the vertical axis shows the ratio of calculated strength to plastic moment strength for the FE analysis and the proposed formula. The ratios for the FE results and the proposed formula are expressed as M_{FEM}/M_p and M_{cr}^*/M_p and are shown in the graphs with a small circles and a broken line, respectively. When both circles and line are closely situated, it indicates that the proposed formula has good accuracy. Keeping in mind this basis for evaluation, the proposed formula provides good overall strength estimates. Note that in Figure 8 (a), there is some scatter in the smaller $\sqrt{M_p/M_{cr}^*}$ region. This is possibly caused by LTB and web shear buckling interaction, which was not directly considered in the proposed formula.

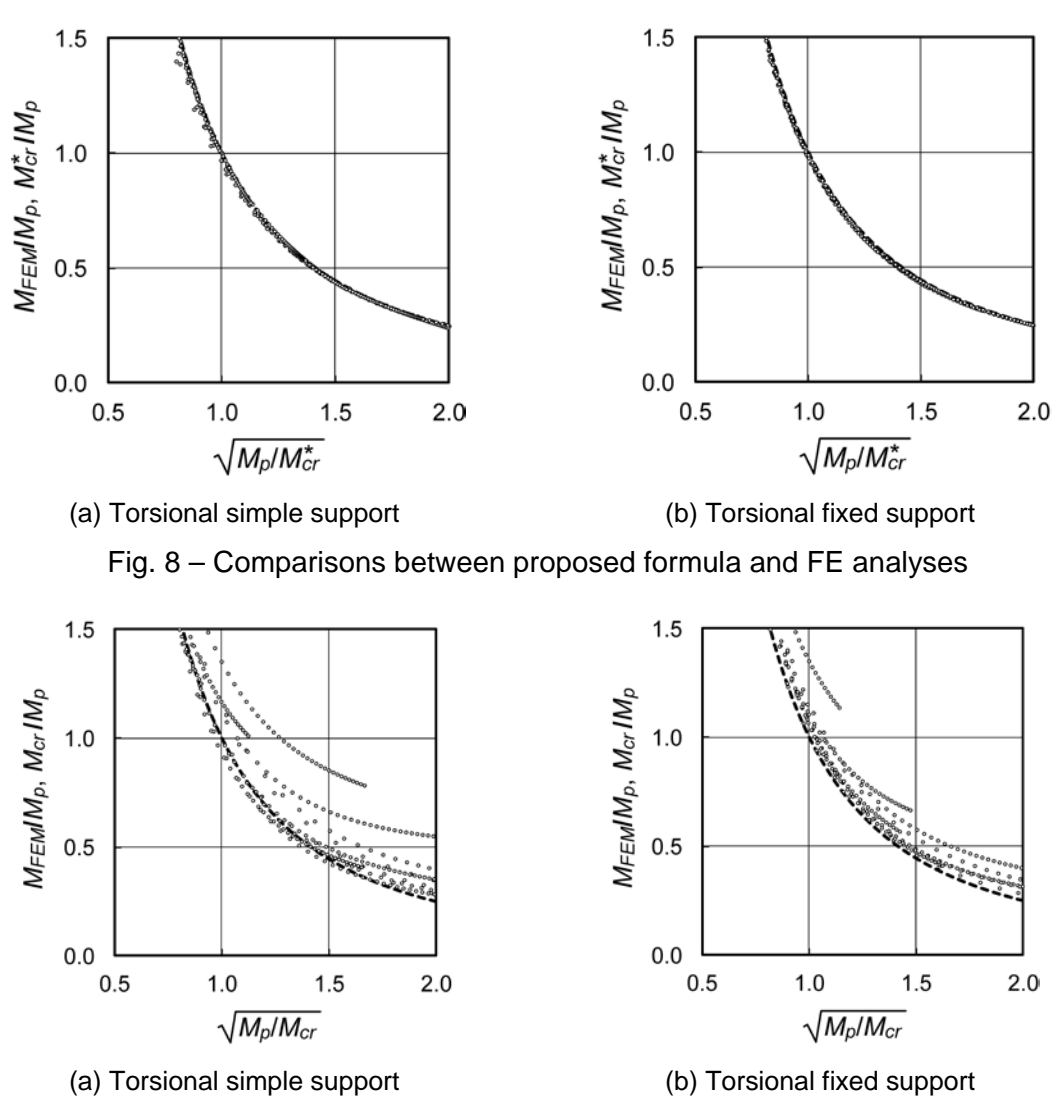


Fig. 9 - Comparison between AISC formula (Yura's formula) and FE analyses

On the other hand, regarding the AISC formula (Yura's formula) given in Eqn. (1), comparisons with the FE analyses are made in Figure 9. Note that Yura's formula was provided primarily for torsional simple support condition, but in this comparison, an effective length factor of 0.5 was applied as an attempt to the torsional fixed support case. Overall, Yura's formula provided conservative strength estimates, but relatively wider scatter was observed for some cases. Although relatively good approximation was provided for uniform bending moment cases, larger scatter was found especially in the cases where the moment gradient was larger (i.e., β was larger), the depth of the steel beam became smaller, and the length of the beam was longer. It is interesting to note that smaller depth and larger length conditions corresponded to the cases where uniform torsion resistant became dominant in comparison with warping torsion resistance. The larger scatter might be caused by the fact that Yura's formula was approximate based on limited numerical solutions. It should be noted that Yura's formula slightly overestimated the cases with β = 3, the largest moment gradient in the calculations. Overall, Figures 8 and 9 show that the proposed formula provided better accuracy than Yura's formula.

COMPARISON BETWEEN PROPOSED FORMULA AND EXPERIMENTAL RESULTS

Since the proposed LTB formula only provided elastic strength, design equations (mapping functions) were needed to consider the effects of inelastic behavior and initial imperfections. Generally, such equations are described as functions of plastic moment, elastic buckling strength and slenderness ratio. In the AISC specification, which is the most widely recognized formula, the unbraced length L_b was used to represent the slenderness ratio. In the proposed buckling formula, however, one might notice that the elastic buckling strength M_{cr}^* was not explicitly expressed as a function of L_b . Therefore, the AISC design equations cannot directly be used for the proposed formula. Based on a Japanese design standard, the following equations were proposed as functions of non-dimensional slenderness ratio $\lambda_b = \sqrt{M_p/M_{cr}^*}$:

(a) When
$$\lambda_b \leq \lambda_p$$
:
$$M_p^* = M_p$$
(30)

(b) When $\lambda_p < \lambda_b \le \lambda_e$:

$$\boldsymbol{M}_{n}^{*} = \left(1 - 0.4 \frac{\lambda_{b} - \lambda_{p}}{\lambda_{e} - \lambda_{p}}\right) \boldsymbol{M}_{p} \tag{31}$$

where

$$\lambda_b = \sqrt{M_p / M_{cr}^*}, \quad \lambda_e = \sqrt{1/0.6}, \quad \lambda_p = 0.6$$
 (32), (33), (34)

(c) When
$$\lambda_b > \lambda_e$$
:
$$M_n^* = M_{cr}^*$$
(35)

In the above equations, M_n^* is the design buckling strength considering the inelastic behavior of the beam. λ_p is the slenderness ratio where M_n^* reaches M_p , and λ_e is the ratio of a transition point between elastic and inelastic buckling. The value of 0.6 for λ_p was assumed on the basis of material and geometrical non-linear buckling analyses separately conducted.

Figure 10 shows a comparison between the experimental data and the design equations given in Eqns. (30) through (35). The horizontal axis represents the non-dimensional slenderness ratio, where M_{cr}^* is given by the proposed formula of Eqn. (13). The vertical axis represents the strength normalized by plastic moment, where the strength is given by the experiments or the

above equations. In Figure 10, elastic buckling strength shown in Eqn. (13) is also indicated as a reference. In calculating M_{cr}^* , the fixed support condition was applied by using Table 3 and the moment gradient parameter β was assumed to be 2, corresponding to a double curvature and an equal end moment condition. Note that setting an appropriate β is relatively difficult because of the beam composite action seen in positive bending. Based on the calculated stresses of the bottom flanges at both ends of the composite beam, $\beta=2$ was approximately assumed for a comparison with the experiments.

As seen in the figure, the design equations are on the safe side against the experimental results, providing with relatively good estimates for

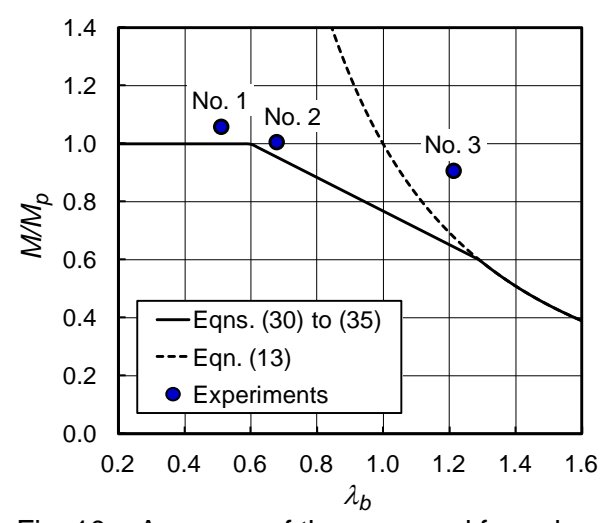


Fig. 10 – Accuracy of the proposed formula

Specimens No. 1 and No. 2, and with a conservative estimate for Specimen No. 3. This conservative estimate may be explained possibly by the following two reasons: One is an additional effect from the rotational restraint at the top of the flange. As seen in Figure 6, the rotational restraint was conservatively neglected in the model. The other is the moment gradient definition for a composite beam. As stated previously, $\beta = 2$ was assumed in calculating M_{cr}^* , but the actual gradient subjected to the steel beam might become larger, resulting in some strength increase. Note that the AISC (Yura's) formula is not shown together in Figure 10, because the torsional fixed support condition seemed to be out of scope for the AISC design

equations. Therefore, a comparison of elastic buckling strength with the same end condition and moment gradient as those in Figure 10 was made in Table 5 between Yura's and the proposed formulae. Yura's formula provided conservative elastic strength estimates.

Table 5 – Accuracy of Yura's formula

Specimen no.	Yura's Mcr /Mp	Proposed M*cr /Mp
No.1	3.26	3.84
No.2	1.89	2.18
No.3	0.63	0.68

CONCLUSIONS

This study aimed to clarify the behavior and design of LTB of an I-shaped steel beam with the top flange continuously restrained laterally using a reinforced concrete floor slab and headed studs. Three sub-assemblage specimens having different flange widths were first tested under horizontal loading applied to the columns. The loading condition was reverse curvature and equal end moment, which is typically seen in seismic design. Through the experiments, it was shown that the floor slab effectively restrained the flexural-torsional buckling for all the cases. An elastic buckling strength formula was then derived for the restrained steel beam based on an energy approach. New displacement functions were introduced so that a closed-form formula was made possible. In comparison with finite element analyses, the accuracy of the proposed formula together with that of the existing AISC formula (Yura's formula) was examined. The comparisons indicated that the proposed formula provided good accuracy while the existing AISC formula had a relatively large scatter for some cases. Finally, the proposed formula was compared with experimental results. In doing so, new design equations to consider the inelastic effect were proposed. The comparison showed that the proposed equations provided reasonably accurate and conservative strength estimates to the experimental results.

REFERENCES

American Institute of Steel Construction (AISC). (2010). Specification for structural steel buildings. Chicago, IL: AISC Committee on Specifications.

Bradford M.A. & Gao, Z. (1992). Distortional buckling solutions for continuous composite beams. *Journal of Structural Engineering* (ASCE). 118 (1). 73-89.

Kimura Y. & Yoshino Y. (2016). Effect of lateral-torsional restraint of continuous braces on lateral buckling strength for H-shaped beams with flexural moment gradient. *Journal of Structural and Construction Engineering*, 81 (726), 1309-1319 (in Japanese).

Trahair, N. S. (1993). Flexural-torsional buckling of structures. Bosa Roca, FL: CRC Press.

Wakabayashi, M. & Nakamura, T. (1973). Numerical analysis of Lateral buckling strength of H-shaped steel beams subjected to end moments and uniformly distributed load. *Transactions of the Architectural Institute of Japan*. 208. 7-13 (in Japanese).

Yura, J. A. (1995). Bracing for stability - State-of-the-Art. *Proceedings of the ASCE Structures Congress XIII.* (pp. 88–103). New York, NY: American Society of Civil Engineers (ASCE).

Ziemian, R. D. (Ed.). (2010). *Guide to stability design criteria for metal structures*, 6th Edition. Hoboken, NJ: John Wiley & Sons.